I&EC research
Industrial & Engineering Chemistry Research

pubs.acs.org/IECR

Article

Microstructure Optimization of the MIP-177-LT Membrane for Highly Efficient Uranium Separation from Seawater

Published as part of Industrial & Engineering Chemistry Research special issue "MOF2024: From Laboratory to Industry".

Yue Zhang, Meixi Yan, Tingting Wang, Sixing Chen, Jie Jiang, Mingming Wu, Shin-ichiro Noro, Xin Zheng, Sujing Wang, Jiaxin Liu, Jing Ma, and Yi Liu*

Cite This: https://doi.org/10.1021/acs.iecr.5c01651

Read Online

ACCESS | Metrics & More | Article Recommendations | SI Supporting Information

ABSTRACT: Although it has been valued as a major chemical separation technology to change the world, high-efficiency separation of UO_2^{2+} from seawater remains a pivotal challenge to date. In this study, we prepared a *c*-oriented MIP-177-LT membrane on a tubular substrate through epitaxial growth. Benefiting from 11 Å sized pores along the *c* axis, the rejection rate of UO_2^{2+} ions reached 98.3%, which was much higher than those of other metal ions (e.g., 4−6% for Na^+, K^+, Ca^{2+}, and Mg^{2+}; 41% for Fe^{3+}). Through combination with 3 Å sized channels along the *b* axis, the water permeance reached as high as 63.4 $L \cdot m^{-2} \cdot h^{-1} \cdot bar^{-1}$, revealing great potential in practical uranium separation from seawater.

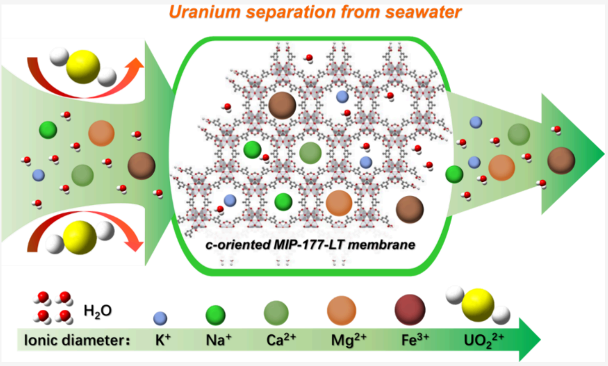

1. INTRODUCTION

To promote the goal of carbon neutrality, nuclear power has been identified as a promising energy source.[1−3] However, land-based uranium fuel reserves are limited to ∼6.3 million tons and will face a severe shortage in less than 100 years.[4−6] Fortunately, there are about 4.5×10^9 tons of uranium resources in seawater,[7,8] providing a solution to the current uranium shortage. Nonetheless, the complicated composition of seawater poses a challenge to high-efficiency uranium purification.[9−12] One the one hand, a large number of interfering metal ions (e.g., Fe^{3+}, Mg^{2+}, Ca^{2+}, Na^+, and K^+) coexist in nature seawater, rendering high-efficiency separation of trace amounts of UO_2^{2+} ions (3.3 ppm) very challenging;[11,13,14] on the other hand, the salinity of seawater (3.2−4.0 wt %) is $\sim 10^6$ times higher than UO_2^{2+} ions,[13,15,16] significantly hindering the efficiency of uranium separation.

Diverse protocols, including adsorption,[11,17−21] photocatalysis,[6,22−28] ion exchange,[29−31] solvent extraction,[32−34] electrochemical precipitation,[35−37] and membrane,[38,39] have been studied for the uranium separation from seawater. Among them, membrane technology has attracted much attention because of the high efficiency, low energy requirement, operation simplicity, and eco-friendliness.[15,16,40] Aiming at achieving high-efficiency uranium separation from seawater, accurate discrimination of UO_2^{2+} ions from coexisting interfering ions (e.g., Fe^{3+}, Mg^{2+}, Ca^{2+}, Na^+, and K^+) has become indispensable. Since hydrated kinetic diameters of hydrated metal ions in seawater are in the order K^+(6.6 Å) < Na^+(7.2 Å) < Ca^{2+}(8.2 Å) < Mg^{2+}(8.6 Å) < Fe^{3+}(9.1 Å) < UO_2^{2+}(11.6 Å), the selection of microporous membranes with pore size ranging between hydrated diameters of UO_2^{2+} ions and other metal ions (e.g., 10−11 Å) is preferred.[41,42] In principle, the rejection rate of UO_2^{2+} ions should be as high as possible (ideally 100%), while that of other metal ions should be as low as possible (ideally, 0%). GO-based membranes have been employed in uranium separation from seawater. The rejection rate of UO_2^{2+} ions in simulated seawater was ∼100%; however, the rejection rate of other ions remained relatively high (>10%); simultaneously, water permeance of GO-based membranes was relatively low, which could be due to the high tortuosity of the pore channels in 2D membranes, resulting in a high diffusion barrier.[43,44] Therefore, both the pore size and preferred orientation of microporous membranes should be deliberately tailored.

Metal−organic frameworks (MOFs), a class of porous crystalline materials composed of regularly arranged metal ions/metal-oxo clusters and organic ligands, have been

Received: April 23, 2025
Revised: June 6, 2025
Accepted: June 20, 2025

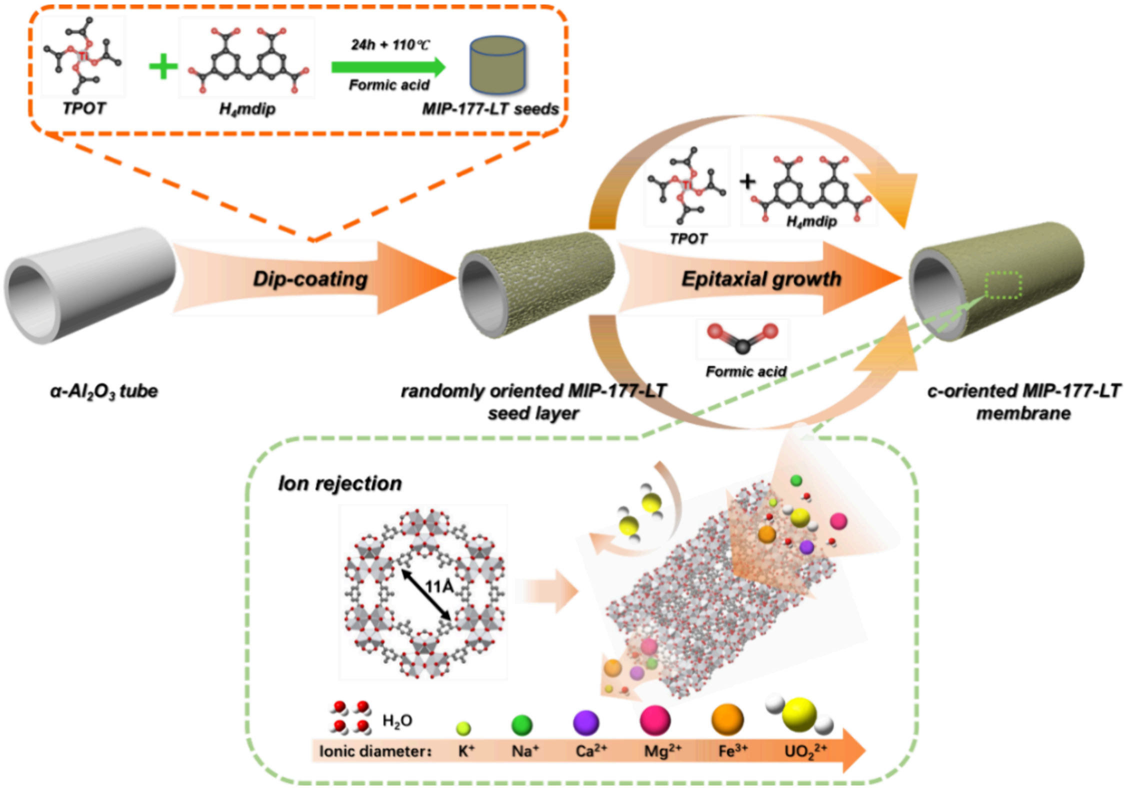

Figure 1. Schematic illustration of the synthesis of the MIP-177-LT membrane toward uranium separation from natural seawater.

regarded as excellent membrane candidates for molecular sieving because of their tunable pore size, rich functional groups, and high surface areas.[4,40,45−48] Among them, MIP-177-LT, which consists of $Ti_{12}O_{15}$ units interconnected by 3,3′,5,5′-tetracarboxydiphenylmethane (H_4mdip) ligands and interconnecting formate groups, features a three-dimensional pore system with 11 Å hexagonal-shaped pores extending along the *c* axis (Figure S3c,d).[49,50] Since its pore size just falls between the kinetic diameters of UO_2^{2+} ions and other smaller-sized metal ions (e.g., Fe^{3+} ions), the fabrication of a preferentially *c*-oriented MIP-177-LT membrane would be promising for high-efficiency uranium separation from seawater; moreover, relying on the coupling effect between the 3 Å sized channel along the *b* axis and the 11 Å sized channel along the *c* axis, versatile water permeation channels can be provided, which is beneficial for achieving higher water permeance.

In this study, we fabricated the highly *c*-orientated MIP-177-LT membrane through epitaxial growth (Figure 1).[51] Since the growth rate of MIP-177-LT crystallites along the *c*-orientation was faster than other orientations, according to the van der Drift evolution principle, MIP-177-LT crystallites evolving along the *c*-direction would prevent the growth of other crystallites along other directions, leading to the formation of a preferentially *c*-oriented MIP-177-LT membrane. Relevant ion rejection experiment data showed that the obtained membrane exhibited a UO_2^{2+} rejection rate of 98.3% with a water permeance of 44.6 L·m^{-2}·h^{-1}·bar^{-1}; in contrast, the rejection rate of M^{n+} (M = K, Na, Ca, and Mg, n = 1 and 2) was below 6%. Of particular note, the Fe^{3+} rejection rate was only 41.4%. To the best of our knowledge, such a large rejection discrepancy between UO_2^{2+} and Fe^{3+} has been rarely reported in the literature.

2. EXPERIMENTAL SECTION

2.1. Preparation of MIP-177-LT Nanoseeds. 5,5′-Methylenediisophthalic acid (H_4mdip, 100 mg, 0.29 mmol, Shanghai Tensus Biotech Co., Ltd.) was added into formic acid (10 mL) and dispersed by sonication at 25 °C for 15 min. Titanium isopropoxide (TPOT, 300 μL, 0.99 mmol) was added dropwise to the above precursor suspension under sonication. Following sonication for 15 min, the above suspension was poured into a 30 mL Teflon-lined autoclave and solvothermally treated at 110 °C for 24 h. After repeated washing with ethanol, the solid product was finally dried in an oven at 60 °C overnight.

2.2. Preparation of the MIP-177-LT Seed Layer. Dip coating was implemented to deposit the MIP-177-LT seed layer. MIP-177-LT seed suspension (4 mg/mL) was prepared by adding 120 mg of MIP-177-LT nanoseeds in 30 mL of MeOH. Subsequently, 20 μL of PVP solution (0.01 mmol/L, solvent is DMF) was added to the suspension and stirred for 3 days before using. Then, a porous α-Al_2O_3 tube was immersed in MIP-177-LT nanoseed suspension for 20 s and slowly lifted out. The operation was repeated twice. Finally, the seed layer was dried at 60 °C for 12 h.

2.3. Preparation of the MIP-177-LT Membrane. H_4mdip (80 mg) was added to 25 mL of formic acid and sonicated for 10 min until complete dissolution of the ligand. Then, 400 μL of TPOT was added to the above precursor suspension under vigorous stirring. After 15 min of sonication, the suspension was transferred to a 60 mL Teflon-lined autoclave in which the MIP-177-LT seed layer was vertically placed. Finally, the Teflon-lined autoclave was treated at 110 °C for 25 h. After cooling, the as-prepared MIP-177-LT membrane was washed with DI water overnight before use.

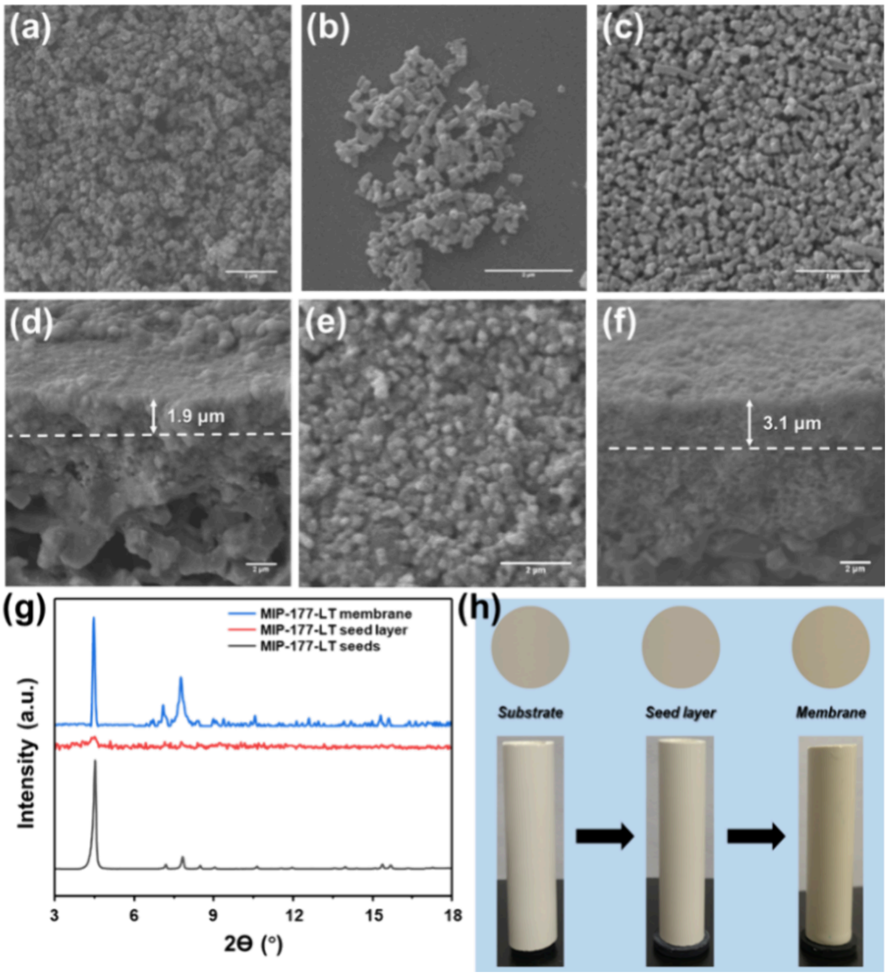

Figure 2. SEM images of (a, b) MIP-177-LT seeds, (c, d) MIP-177-LT seed layer, and (e, f) MIP-177-LT membrane. (g) XRD patterns of MIP-177-LT seeds, seed layer, and membrane. (h) digital photos of the α-Al_2O_3 substrate, MIP-177-LT seed layer, and MIP-177-LT membrane. Scale bars: 2 μm.

3. RESULTS AND DISCUSSION

3.1. Preparation of MIP-177-LT Seeds.

MIP-177-LT nanoseeds were synthesized in the first step, which could be facilely prepared through reported literature.[52] As shown in Figure 2a, the obtained rod-shaped seeds exhibited an aspect ratio of ∼1.6 (Figure 2b) with size distribution ranging between 250 and 350 nm (Figure S4a,b). Relevant XRD patterns were consistent with the standard MIP-177-LT phase (Figure S5). N_2 adsorption/desorption isotherms indicated that their BET surface areas and micropore volume reached 526.98 $m^2 \cdot g^{-1}$ and 0.3812 $cm^3 \cdot g^{-1}$ (Figure S6), respectively, which were comparable with those in the reported literature.

Considering the high salinity, complex composition, and varying temperature of seawater, the robustness of MIP-177-LT crystallites in aqueous solution was further evaluated under varying pH values (1−4 and 10) and temperatures. As shown in Figure S7, the morphology of MIP-177-LT crystallites did not change under the above harsh conditions. XRD patterns and FT-IR spectra showed that there was no variation in phase purity and functionality (Figures S8 and S9), while TGA data showed that there was no significant weight loss of up to 400 °C (Figure S10). Therefore, the obtained MIP-177-LT crystallites exhibited excellent chemical and thermal stability, which was beneficial to withstand long-term exposure to natural seawater.

3.2. Preparation of the MIP-177-LT Seed Layer and Relevant Membrane.

Subsequently, we attempted to deposit a uniform MIP-177-LT seed layer through dip coating. The results showed that the addition of PVP represented the key factor to maintain the uniformity of the MIP-177-LT seed layer. Obviously, the addition of PVP in seed suspension weakened mutual interactions between adjacent MIP-177-LT seeds, resulting in enhanced dispersion in suspension.[53,54] As shown in Figure S11, MIP-177-LT nanoseeds were uniformly deposited on porous α-Al_2O_3 tubes upon maintaining a seed solution concentration of 2−5 mg/mL; nonetheless, further increasing seed concentration would lead to severe aggregation in the seed layer. As shown in Figure 2c,d, the thickness of the randomly oriented MIP-177-LT seed layer reached 1.9 μm.

The next step referred to epitaxial growth for sealing the open space in the seed layer. According to the van der Drift evolution mechanism, since the growth rate of MIP-177-LT crystallites along the *c*-orientation was faster than other orientations, when they met, MIP-177-LT crystallites growing closer to the *c*-orientation would prevent further growth of the ones evolving along other orientations. Eventually, bc-/ac-faces of MIP-177-LT crystallites tended to arrange in a direction perpendicular to the substrate surface, which led to the formation of the preferentially *c*-orientated MIP-177-LT membrane.[51,52] Our results revealed that increasing the

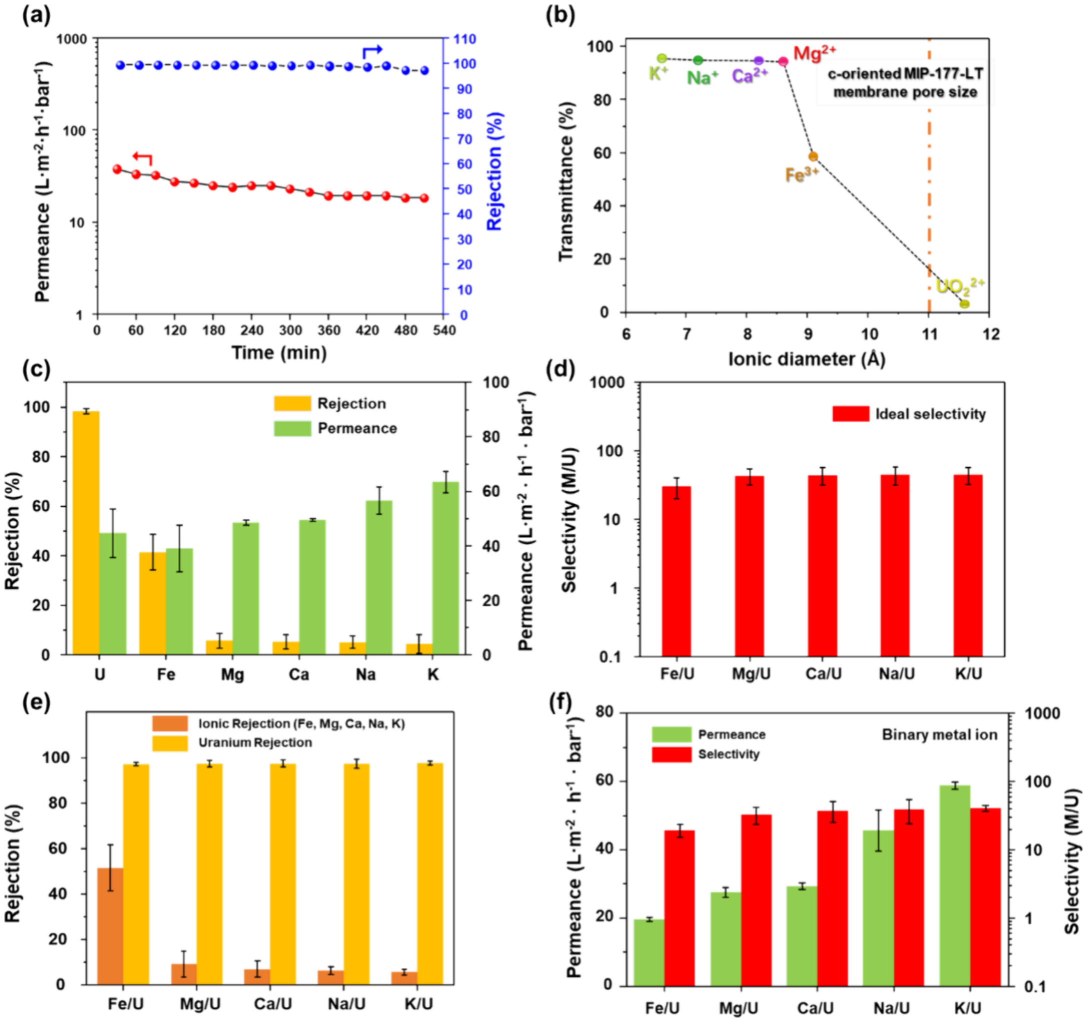

Figure 3. (a) Long-term CR rejection test of the MIP-177-LT membrane. (b) Metal ion transmission rate of the MIP-177-LT membrane as a function of the ionic diameter. (c) Single metal ion separation performance of the MIP-177-LT membrane. (d) Ideal selectivity of M^{n+} (n = 1, 2, and 3)/UO_2^{2+} ion pairs. (e) Binary metal ion separation performance of the MIP-177-LT membrane. (f) SF of binary M^{n+} (n = 1, 2, and 3)/UO_2^{2+} ion pairs.

H_4mdip concentration (≤4 mg/mL) was beneficial for increasing the degree of *c*-orientation of MIP-177-LT membranes (Figure S12).[55] Under optimized conditions, a well-intergrown MIP-177-LT membrane with a thickness of 3.1 μm was obtained (Figure 2e,f). The cross-sectional image showed that the membrane thickness was increased by 63.15% compared with the seed layer, revealing that the epitaxial growth along the out-of-plane direction was triggered to a large extent.[56−58] The relevant XRD pattern exhibited a significant diffraction peak at a 2θ value of 7.1°, corresponding to the (001) plane of the MIP-177-LT phase (Figure 2g). The crystallographic preferred orientation (CPO) index has been widely employed to quantify the degree of preferred orientation of crystallites in the membrane. In this study, the $CPO_{(001)/(100)}$ index, in which I_M and I_P belonged to the intensity of (001) and (100) plane reflections, respectively, was employed to evaluate the degree of the *c*-preferred orientation of the MIP-177-LT membranes (shown in Figure S8). Our results indicated that compared with the MIP-177-LT seed layer, the $CPO_{(001)/(100)}$ index of the MIP-177-LT membrane significantly increased to 8.4, indicating the dominance of the preferred *c*-orientation of MIP-177-LT crystallites in the membrane, which was beneficial for the concurrent increase in rejection rate and water permeance due to the appropriate pore size and minimized diffusion path length.

3.3. Ion Rejection Test of the MIP-177-LT Membrane.

Before the ion rejection test, the continuity of our membrane was assessed with a 25 Å sized Congo Red (CR, Figure S14) rejection test. A CR rejection rate of ∼99% was achieved with a water permeance of 37 $L\cdot m^{-2}\cdot h^{-1}\cdot bar^{-1}$, indicating the existence of a few grain boundary defects in the membrane (Figure 3a). Subsequently, the ion rejection capacity of the obtained MIP-177-LT membrane was evaluated. We first measured the single ion rejection capacity of the membrane. Since the pore size of MIP-177-LT in the *c*-axis direction fell between UO_2^{2+} ions and other smaller-sized metal ions, an accurate screening of UO_2^{2+} ions could be realized (Figure 3b). As shown in Figure 3c, the rejection rate of UO_2^{2+} ions of our membrane reached 98.3%, which was much higher than those of K^+ (4.5%), Na^+ (5.1%), Ca^{2+} (5.3%), Mg^{2+} (5.7%), and Fe^{3+} ions (41.4%), implying that size-based exclusion represented the dominant mechanism for metal ion rejection; correspondingly, the ideal selectivities of K^+/UO_2^{2+}, Na^+/UO_2^{2+}, Ca^{2+}/UO_2^{2+}, Mg^{2+}/UO_2^{2+}, and Fe^{3+}/UO_2^{2+} ion pairs reached 44.5, 44.4, 43.9, 42.8, and 29.86, respectively (Figure 3d). It should be noted that in sharp contrast to the high rejection rate of

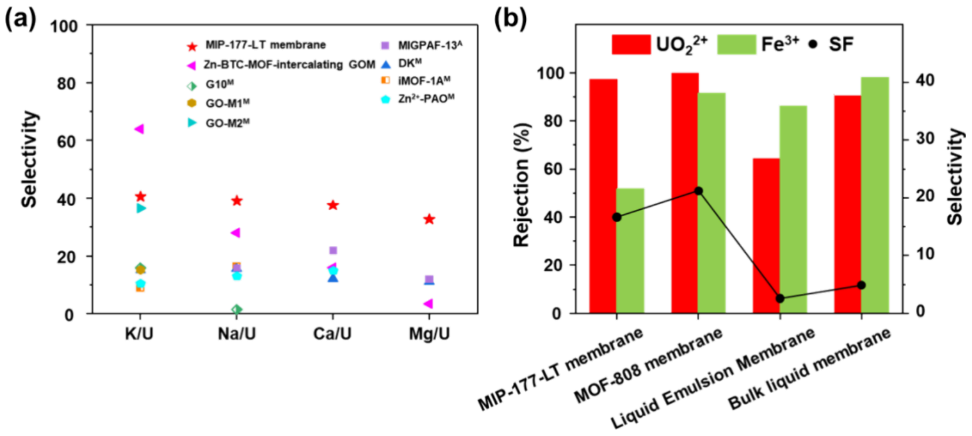

Figure 4. (a) Comparison of the selectivity of binary M^{n+} (n = 1 and 2)/UO_2^{2+} ion pairs of the MIP-177-LT membrane with other materials (Tables S1 and S2). (b) Comparison of rejection rates of UO_2^{2+} and Fe^{3+} ions as well as the SF of binary Fe^{3+}/UO_2^{2+} ion pairs of the MIP-177-LT membrane with other materials reported in the literature (Table S3).

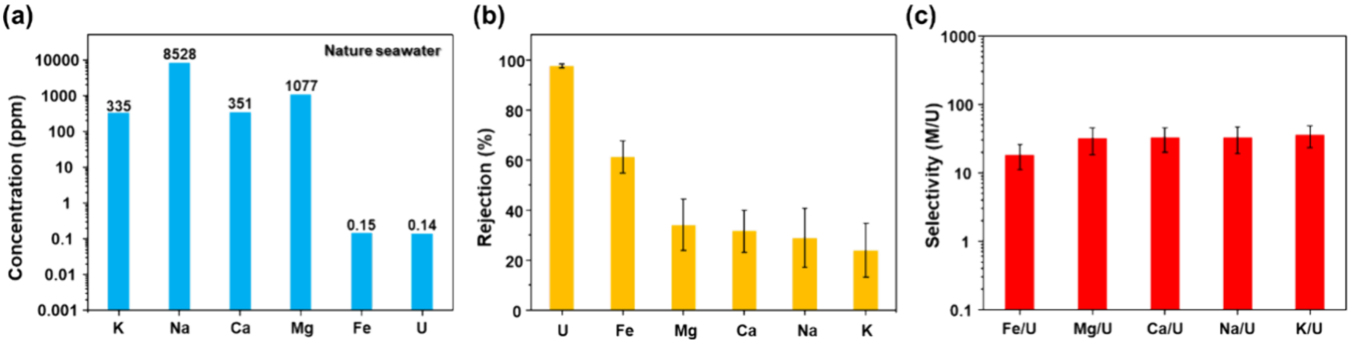

Figure 5. Uranium separation capacity of the MIP-177-LT membrane under natural seawater conditions. (a) Concentrations of the main metal ions from the Yellow Sea at Dalian; (b) rejection rates of various metal ions; (c) selectivity of M^{n+} (n = 1, 2, and 3)/UO_2^{2+} ion pairs under natural seawater conditions.

UO_2^{2+} ions, rejection rates of M^+ and M^{2+} ions were remarkably lower (<6%), which was advantageous for accurately screening UO_2^{2+} ions from other high-concentration interfering metal ions. We also noticed that there was a remarkable difference between rejection rates of Fe^{3+} and UO_2^{2+} ions. We have recently reported the preparation of MOF-808 membranes with the rejection rate of Fe^{3+} ions reaching 98.3%, which was remarkably higher than that of MIP-177-LT membranes.[59] Such a large discrepancy in rejection rates of Fe^{3+} ions could be attributed to the slightly larger pore size of the MIP-177-LT membrane, resulting in a higher diffusion rate of Fe^{3+} ions through the membrane with negligible influence on the Fe^{3+}/UO_2^{2+} selectivity; simultaneously, the water permeance of the K^+ ion-containing solution reached 63.4 $L \cdot m^{-2} \cdot h^{-1} \cdot bar^{-1}$. As far as we know, this represented the highest value reported in the literature for pure MOF membranes, which could be attributed to (i) minimized diffusion path length in the membrane, (ii) versatile channels enabling fast permeation of water molecules, and (iii) hydrophilicity of the MIP-177-LT membrane surface (Figure S15). As expected, the water permeance generally decreased with increasing hydrated kinetic diameters of metal ions, which could be rationally interpreted by the size-exclusion effect (Figure 3c).

We further evaluated the binary metal ion separation capacity of the obtained MIP-177-LT membrane. As shown in Figure 3c, compared with single metal ions, there was a slight increase in rejection rate in the presence of UO_2^{2+} ions. For instance, the rejection rate of K^+ ions reached 5.7% in the presence of UO_2^{2+} ions, which was slightly higher than that of single K^+ ions (Figure 3e). This may be due to the strong coupling effect between metal ions and competitive diffusion in the channel, giving rise to higher ion-permeable free energy barriers.[60,61] To be specific, the separation factors (SFs) of K^+/UO_2^{2+}, Na^+/UO_2^{2+}, Ca^{2+}/UO_2^{2+}, Mg^{2+}/UO_2^{2+}, and Fe^{3+}/UO_2^{2+} ion pairs reached 40.6, 39.1, 37.7, 32.7, and 19.5, respectively (Figure 3f) with water permeance largely unchanged (58.89, 45.64, 29.30, 27.52, and 19.63 $L \cdot m^{-2} \cdot h^{-1} \cdot bar^{-1}$) (Figure 3e). It should be noted that in comparison with the literature (Figure 4a), our membrane displayed efficient UO_2^{2+} interception and screening precision toward versatile metal ions (M^{n+}/UO_2^{2+}, n = 1 and 2) while maintaining high water permeance, which had been rarely reported in the literature (Tables S1 and S2); moreover, in comparison with the literature, our membrane exhibited the largest difference between rejection rates of Fe^{3+} and UO_2^{2+} ions (Figure 4b and Table S3).

Targeting practical applications, we further investigated the uranium rejection capacity of the MIP-177-LT membrane under natural seawater conditions. According to the literature, uranium in natural seawater mainly exists in the form of UO_2^{2+} ions.[11,62,63] Concentrations of major metal ions in the Yellow Sea are as follows (Figure 5a): Na^+ (~8528 ppm) > Mg^{2+} (~1077 ppm) > K^+ (~335 ppm) ~ Ca^{2+} (~351 ppm) > Fe^{3+} (~0.15 ppm) > UO_2^{2+} (~0.14 ppm). Our results showed that the uranium rejection rate reached 97.6%, which was comparable to the rejection rate of single UO_2^{2+} ions, while rejection rates of other smaller-sized metal ions only slightly increased, indicating a negligible influence on the separation efficiency (Figure 5b). Correspondingly, our membrane exhibited satisfying selectivity toward K^+/UO_2^{2+} (36.2), Na^+/UO_2^{2+} (33.1), Ca^{2+}/UO_2^{2+} (33.0), Mg^{2+}/UO_2^{2+} (32.1), and Fe^{3+}/UO_2^{2+} (18.6) ion pairs with a water permeance of 14.43 $L \cdot m^{-2} \cdot h^{-1} \cdot bar^{-1}$ (Figure 5c), showing great promise for high-efficiency uranium separation from natural seawater.

4. CONCLUSIONS

In this study, a preferentially *c*-oriented MIP-177-LT membrane was fabricated on a porous α-Al_2O_3 tube. Relying on 11 Å sized channels arranged along the *c* axis, the obtained membrane achieved a rejection rate of 98% for UO_2^{2+} ions. In contrast, rejection rates as low as <6% were achieved in terms of small-sized hydrated monovalent and divalent metal ions; simultaneously, the largest difference between rejection rates of Fe^{3+} and UO_2^{2+} ions in comparison with the literature was achieved in terms of pure MOF membranes. Under natural seawater conditions, the rejection rate of UO_2^{2+} ions reached 97.6% with a water permeance of 14.4 $L \cdot m^{-2} \cdot h^{-1} \cdot bar^{-1}$, holding great promise for practical uranium separation from nature seawater with balanced UO_2^{2+} selectivity and water permeance.

■ ASSOCIATED CONTENT

Supporting Information

The Supporting Information is available free of charge at https://pubs.acs.org/doi/10.1021/acs.iecr.5c01651.

> Additional experimental details, experimental reagents, detailed characterizations of MIP-177-LT powders and membranes, and relevant test details (PDF)

■ AUTHOR INFORMATION

Corresponding Author

Yi Liu − *State Key Laboratory of Fine Chemicals, Frontiers Science Center for Smart Materials, School of Chemical Engineering and Dalian Key Laboratory of Membrane Materials and Membrane Processes, Dalian University of Technology, Dalian 116024, China;* orcid.org/0000-0002-2073-4832; Email: diligenliu@dlut.edu.cn

Authors

Yue Zhang − *State Key Laboratory of Fine Chemicals, Frontiers Science Center for Smart Materials, School of Chemical Engineering, Dalian University of Technology, Dalian 116024, China;* orcid.org/0009-0001-6712-2729

Meixi Yan − *State Key Laboratory of Fine Chemicals, Frontiers Science Center for Smart Materials, School of Chemical Engineering, Dalian University of Technology, Dalian 116024, China*

Tingting Wang − *State Key Laboratory of Fine Chemicals, Frontiers Science Center for Smart Materials, School of Chemical Engineering, Dalian University of Technology, Dalian 116024, China*

Sixing Chen − *State Key Laboratory of Fine Chemicals, Frontiers Science Center for Smart Materials, School of Chemical Engineering, Dalian University of Technology, Dalian 116024, China*

Jie Jiang − *State Key Laboratory of Fine Chemicals, Frontiers Science Center for Smart Materials, School of Chemical Engineering, Dalian University of Technology, Dalian 116024, China*

Mingming Wu − *State Key Laboratory of Fine Chemicals, Frontiers Science Center for Smart Materials, School of Chemical Engineering, Dalian University of Technology, Dalian 116024, China*

Shin-ichiro Noro − *Faculty of Environmental Earth Science, Hokkaido University, Sapporo 060-0810, Japan;* orcid.org/0000-0003-4757-4741

Xin Zheng − *Faculty of Environmental Earth Science, Hokkaido University, Sapporo 060-0810, Japan;* orcid.org/0000-0003-4737-6083

Sujing Wang − *Hefei National Research Center for Physical Sciences at the Microscale, Suzhou Institute for Advanced Research, and Hefei National Laboratory, CAS Key Laboratory of Microscale Magnetic Resonance, University of Science and Technology of China, Hefei 230026, China;* orcid.org/0000-0003-0942-2907

Jiaxin Liu − *China Nuclear Power Engineering Company Limited, Beijing 100840, China*

Jing Ma − *China Nuclear Power Engineering Company Limited, Beijing 100840, China*

Complete contact information is available at: https://pubs.acs.org/10.1021/acs.iecr.5c01651

Author Contributions

The manuscript was written through contributions of all authors. All authors have given approval to the final version of the manuscript. Y.Z. performed the major experiments and analyzed the experimental data. M.Y. and T.W. helped with the experiments on uranium rejection under natural seawater conditions. S.C. and J.J. helped with the experiments on CR rejection. M.W. helped with the analysis of experimental data. S.W., S.-i.N., and X.Z. helped with the compilation of the manuscript. J.L. and J.M. helped with the hydrophilic angle measurements and Congo Red dye diagram drawing. Y.L. and Y.Z. cowrote the manuscript with contributions from all authors.

Notes

The authors declare no competing financial interest.

■ ACKNOWLEDGMENTS

The authors are grateful to fundings from the National Natural Science Foundation of China (22478056), Liaoning Province Funds for Distinguished Young Scholars (2024JH3/50100002), Science Fund for Creative Research Groups of the National Natural Science Foundation of China (22021005), Liaoning Binhai Laboratory (LBLG-2024-07), State Key Laboratory of Catalysis (2024SKL-A-003), National Key Research and Development Program of China (2023YFB3810700), Science and Technology Innovation Fund of Dalian (2024JJ12GX027), and Fundamental Research Funds for the Central Universities (DUT22LAB602).

■ REFERENCES

(1) Prasad, T. L.; Saxena, A. K.; Tewari, P. K.; Sathiyamoorthy, D. An engineering scale study on radiation grafting of polymeric adsorbents for recovery of heavy metal ions from seawater. *Nucl. Eng. Technol.* **2009**, *41* (8), 1101−1108.

(2) Zeyu, L.; Yi, X.; Yifan, W.; Tongyang, H. U.; Gang, Y. E.; Jing, C. Recent advances in sorbent materials for uranium extraction from seawater. *J. Tsinghua Univ. Sci. Technol.* **2021**, *61* (4), 279−301.

(3) Dan, W. Interpretation of the 13th five-year development plan in support of nuclear power development. *Chin. Nuclear Power* **2017**, *10* (2), 157−160.

(4) Li, J.; Tuo, K.; Fan, C.; Liu, G.; Pu, S.; Li, Z. Hierarchical porous amidoximated metal-organic framework for highly efficient uranium extraction. *Small* **2024**, *20* (13), No. 2306545.

(5) Ding, L.; Wan, X.; Zheng, B.; Dang, Z.; Zhang, S.; Zhang, L. One-pot synthesis of a graphene oxide-supported TixAl1−xoy-based material modified with amidoxime for highly efficient uranium(VI) adsorption. *J. Mater. Chem. A* **2024**, *12* (14), 8381−8391.

(6) Yu, F.; Li, C.; Li, W.; Yu, Z.; Xu, Z.; Liu, Y.; Wang, B.; Na, B.; Qiu, J. Π-skeleton tailoring of olefin-linked covalent organic frameworks achieving low exciton binding energy for photo-enhanced uranium extraction from seawater. *Adv. Funct. Mater.* **2024**, *34* (1), No. 2307230.

(7) Abney, C. W.; Mayes, R. T.; Saito, T.; Dai, S. Materials for the recovery of uranium from seawater. *Chem. Rev.* **2017**, *117* (23), 13935−14013.

(8) Zhao, C. X.; Liu, J. N.; Li, B. Q.; Ren, D.; Chen, X.; Yu, J.; Zhang, Q. Multiscale construction of bifunctional electrocatalysts for long-lifespan rechargeable zinc−air batteries. *Adv. Funct. Mater.* **2020**, *30* (36), No. 2003619.

(9) Wu, Y.; Xie, Y.; Liu, X.; Li, Y.; Wang, J.; Chen, Z.; Yang, H.; Hu, B.; Shen, C.; Tang, Z.; et al. Functional nanomaterials for selective uranium recovery from seawater: material design, extraction properties and mechanisms. *Coord. Chem. Rev.* **2023**, *483*, No. 215097.

(10) Singh, B. K.; Asim, M.; Salkenova, Z.; Pak, D.; Um, W. Engineered sorbents for selective uranium sequestration from seawater. *ACS ES&T water* **2024**, *4* (2), 325−345.

(11) Song, Y.; Deng, B.; Wang, K.; Zhang, Y.; Gao, J.; Cheng, X. Highly-efficient adsorbent materials for uranium extraction from seawater. *Journal of environmental chemical engineering* **2024**, *12* (5), No. 113967.

(12) Krestou, A.; Panias, D. Uranium (VI) speciation diagrams in the UO22+/CO32-/h2o system at 25°c. *Eur. J. Miner. Process. Environ. Prot.* **2004**, *4* (2), 113−129.

(13) Zhang, D.; Fang, L.; Liu, L.; Zhao, B.; Hu, B.; Yu, S.; Wang, X. Uranium extraction from seawater by novel materials: a review. *Sep. Purif. Technol.* **2023**, *320*, No. 124204.

(14) Wang, W.; Yang, K.; Zhu, Q.; Zhang, T.; Guo, L.; Hu, F.; Zhong, R.; Wen, X.; Wang, H.; Qi, J. MOFs-based materials with confined space: opportunities and challenges for energy and catalytic conversion. *Small* **2024**, *20* (37), No. 2311449.

(15) Xing, C.; Bernicot, B.; Arrachart, G.; Pellet-Rostaing, S. Application of ultra/nano filtration membrane in uranium rejection from fresh and salt waters. *Sep. Purif. Technol.* **2023**, *314*, No. 123543.

(16) Endrizzi, F.; Leggett, C. J.; Rao, L. Scientific basis for efficient extraction of uranium from seawater. I: understanding the chemical speciation of uranium under seawater conditions. *Ind. Eng. Chem. Res.* **2016**, *55* (15), 4249−4256.

(17) Witono, A. I.; Zheng, X.; Saito, Y.; Noro, S. Shaping of metal−organic framework using chitosan and triphosphate cross-linker. *Chem. Lett.* **2024**, *53* (4), No. upae050.

(18) Kuo, L.; Pan, H.; Wai, C. M.; Byers, M. F.; Schneider, E.; Strivens, J. E.; Janke, C. J.; Das, S.; Mayes, R. T.; Wood, J. R.; et al. Investigations into the reusability of amidoxime-based polymeric adsorbents for seawater uranium extraction. *Ind. Eng. Chem. Res.* **2017**, *56* (40), 11603−11611.

(19) Li, Y.; Zheng, Y.; Ahamd, Z.; Zhu, L.; Yang, J.; Chen, J.; Zhang, Z. Strategies for designing highly efficient adsorbents to capture uranium from seawater. *Coord. Chem. Rev.* **2023**, *491*, No. 215234.

(20) Chang, X.; Hu, P.; Liu, H.; Lv, Z.; Yang, J.; Wang, J.; Li, Z.; Qian, L.; Wu, W. ZIF-8 modified graphene oxide/sodium alginate 3d elastic spheres for uranium trapping in seawater. *Desalination* **2023**, *549*, No. 116371.

(21) Ye, X.; Chi, R.; Wu, Z.; Chen, J.; Lv, Y.; Lin, C.; Liu, Y.; Luo, W. A biomass fiber adsorbent grafted with phosphate/amidoxime for efficient extraction of uranium from seawater by synergistic effect. *J. Environ. Manage.* **2023**, *337*, No. 117658.

(22) Zhao, S.; Feng, T.; Cao, M.; Liu, T.; Yuan, Y.; Wang, N. Ferrocene-based 2d metal−organic framework nanosheet for highly efficient photocatalytic seawater uranium recovery. *Chem. Eng. J.* **2024**, *498*, No. 155228.

(23) Liu, T.; Gu, A.; Wei, T.; Chen, M.; Guo, X.; Tang, S.; Yuan, Y.; Wang, N. Ligand-assistant iced photocatalytic reduction to synthesize atomically dispersed cu implanted metal-organic frameworks for photo-enhanced uranium extraction from seawater. *Small* **2023**, *19* (26), No. e2208002.

(24) Chen, C.; Fei, L.; Wang, B.; Xu, J.; Li, B.; Shen, L.; Lin, H. MOF-based photocatalytic membrane for water purification: a review. *Small* **2024**, *20* (1), No. 2305066.

(25) Ma, X.; Meihaus, K. R.; Yang, Y.; Zheng, Y.; Cui, F.; Li, J.; Zhao, Y.; Jiang, B.; Yuan, Y.; Long, J. R.; et al. Photocatalytic extraction of uranium from seawater using covalent organic framework nanowires. *J. Am. Chem. Soc.* **2024**, *146* (33), 23566−23573.

(26) Wang, W.; Luo, Q.; Li, J.; Li, Y.; Wu, R.; Li, Y.; Huo, X.; Wang, N. Single-atom tungsten engineering of MOFs with biomimetic antibiofilm activity toward robust uranium extraction from seawater. *Chem. Eng. J.* **2022**, *431*, No. 133483.

(27) Zhang, B.; Shan, X.; Yu, J.; Zhang, H.; Tawfik Alali, K.; Liu, Q.; Zhu, J.; Yu, J.; Liu, J.; Li, R.; et al. Facile synthesis of TiO2-PAN photocatalytic membrane with excellent photocatalytic performance for uranium extraction from seawater. *Sep. Purif. Technol.* **2024**, *328*, No. 125026.

(28) Yu, F.; Zhu, Z.; Wang, S.; Peng, Y.; Xu, Z.; Tao, Y.; Xiong, J.; Fan, Q.; Luo, F. Tunable perylene-based donor-acceptor conjugated microporous polymer to significantly enhance photocatalytic uranium extraction from seawater. *Chem. Eng. J.* **2021**, *412*, No. 127558.

(29) Park, Y. S.; Lee, J.; Jang, M. J.; Yang, J.; Jeong, J.; Park, J.; Kim, Y.; Seo, M. H.; Chen, Z.; Choi, S. M. High-performance anion exchange membrane alkaline seawater electrolysis. *J. Mater. Chem. A* **2021**, *9* (15), 9586−9592.

(30) Li, H.; Chen, S.; Song, Y.; Ding, H.; Li, Z.; Wu, H.; Wang, F.; Li, H.; Gao, Z.; Wang, H. Preparation of antibioadhering materials containing quaternary phosphonium salt for uranium extraction from seawater. *ACS Appl. Polym. Mater.* **2024**, *6* (7), 3796−3804.

(31) Foster, R. I.; Amphlett, J. T. M.; Kim, K.; Kerry, T.; Lee, K.; Sharrad, C. A. SOHIO process legacy waste treatment: uranium recovery using ion exchange. *J. Ind. Eng. Chem.* **2020**, *81*, 144−152.

(32) Jegan, G.; Sreenivasulu, B.; Suresh, A.; Brahmananda Rao, C. V. S.; Sivaraman, N.; Gopakumar, G. Experimental and theoretical studies on solvent extraction of uranium(VI) with hexapropyl and hexabutyl phosphoramide extractants. *Solvent Extr. Ion Exch.* **2022**, *40* (3), 312−332.

(33) Abdeshahi, A.; Sadeghi, M. H.; Ghoddocy Nejad, D.; Habibi Zare, M.; Outokesh, M. Recovery of uranium from phosphate ore of iran mine: part II- solvent extraction of uranium from wet-process phosphoric acid. *Nucl. Eng. Des.* **2024**, *421*, No. 113093.

(34) Tsutsui, N.; Ban, Y.; Sagawa, H.; Ishii, S.; Matsumura, T. Solvent extraction of uranium with n, n -di(2-ethylhexyl)octanamide from nitric acid medium. *Solvent Extr. Ion Exch.* **2017**, *35* (6), 439−449.

(35) Liu, C.; Hsu, P.; Xie, J.; Zhao, J.; Wu, T.; Wang, H.; Liu, W.; Zhang, J.; Chu, S.; Cui, Y. A half-wave rectified alternating current electrochemical method for uranium extraction from seawater. *Nat. Energy* **2017**, *2* (4), 17007.

(36) Chi, F.; Zhang, S.; Wen, J.; Xiong, J.; Hu, S. Highly efficient recovery of uranium from seawater using an electrochemical approach. *Ind. Eng. Chem. Res.* **2018**, *57* (23), 8078−8084.

(37) Feng, H.; Dong, H.; He, P.; He, J.; Hu, E.; Qian, Z.; Li, J.; Li, J.; Zhu, W.; Chen, T. Nickel single atom mediated phosphate functionalization of moss derived biochar effectively enhances electrochemical uranium extraction from seawater. *J. Mater. Chem. A* **2024**, *12* (13), 7896−7905.

(38) Zhu, L.; Zhang, C.; Ma, F.; Bi, C.; Zhu, R.; Wang, C.; Wang, Y.; Liu, L.; Dong, H. Hierarchical self-assembled polyimide microspheres functionalized with amidoxime groups for uranium-containing

https://doi.org/10.1021/acs.iecr.5c01651

wastewater remediation. *ACS Appl. Mater. Interfaces* **2023**, *15* (4), 5577−5589.

(39) Cai, W.; Wang, Y.; Chen, L.; Luo, Q.; Xiong, L.; Zhang, Z.; Xu, L.; Cao, X.; Liu, Y. High-efficiency adsorptive removal of u(VI) on magnetic mesoporous carbon/sr-doped hydroxyapatite composites. *Colloids Surf., A* **2024**, *683*, No. 132975.

(40) Mo, B.; Zhang, Y.; Liu, G.; Liu, G.; Jin, W. Recent progress of metal-organic framework membranes for mono/divalent ions separation. *CIESC J.* **2024**, *75* (4), 1183−1197.

(41) Tansel, B.; Sager, J.; Rector, T.; Garland, J.; Strayer, R. F.; Levine, L.; Roberts, M.; Hummerick, M.; Bauer, J. Significance of hydrated radius and hydration shells on ionic permeability during nanofiltration in dead end and cross flow modes. *Sep. Purif. Technol.* **2006**, *51* (1), 40−47.

(42) Tansel, B. Significance of thermodynamic and physical characteristics on permeation of ions during membrane separation: hydrated radius, hydration free energy and viscous effects. *Sep. Purif. Technol.* **2012**, *86*, 119−126.

(43) Kitagawa, S.; Kitaura, R.; Noro, S. Functional porous coordination polymers. *Angew. Chem., Int. Ed. Engl.* **2004**, *43* (18), 2334−2375.

(44) Zhao, L.; Ren, Y.; Shi, X.; Liu, H.; Yu, Z.; Gao, J.; Zhao, J. Unveiling the unexpected sinking and embedding dynamics of surface supported mo/s clusters on 2d MoS2 with active machine learning. *Smart Molecules* **2025**, *3* (1), No. e20240018.

(45) Koros, W. J.; Zhang, C. Materials for next-generation molecularly selective synthetic membranes. *Nat. Mater.* **2017**, *16* (3), 289−297.

(46) Park, H. B.; Kamcev, J.; Robeson, L. M.; Elimelech, M.; Freeman, B. D. Maximizing the right stuff: the trade-off between membrane permeability and selectivity. *Science* **2017**, *356* (6343), No. eaab0530.

(47) Xia, T.; Wu, Y.; Ji, T.; Hu, W.; Yu, K.; He, X.; Yin, B. H.; Liu, Y. Mixed-matrix membranes incorporating hierarchical ZIF-8 towards enhanced CO2 /n2 separation. Smart. *Molecules* **2025**, No. e20240066.

(48) Lee, D.; Lee, S.; Choi, I.; Kim, M. Positional functionalizations of metal−organic frameworks through invasive ligand exchange and additory MOF-on-MOF strategies: a review. *Smart Molecules* **2024**, *2* (2), No. e20240002.

(49) Esposito, E.; Carta, M.; Fuoco, A.; Monteleone, M.; Comesaña-Gándara, B.; Gkaniatsou, E.; Sicard, C.; Wang, S.; Serre, C.; Mckeown, N. B.; et al. Single and mixed gas permeability studies on mixed matrix membranes composed of MIL-101(cr) or MIL-177(ti) and highly permeable polymers of intrinsic microporosity. *J. Membr. Sci.* **2024**, *697*, No. 122475.

(50) Wang, S.; Kitao, T.; Guillou, N.; Wahiduzzaman, M.; Martineau-Corcos, C.; Nouar, F.; Tissot, A.; Binet, L.; Ramsahye, N.; Devautour-Vinot, S.; et al. A phase transformable ultrastable titanium-carboxylate framework for photoconduction. *Nat. Commun.* **2018**, *9* (1), 1660.

(51) Li, Y.; Bux, H.; Feldhoff, A.; Li, G.; Yang, W.; Caro, J. Controllable synthesis of metal-organic frameworks: from MOF nanorods to oriented MOF membranes. *Adv. Mater.* **2010**, *22* (30), 3322−3326.

(52) Chen, S.; Wahiduzzaman, M.; Ji, T.; Liu, Y.; Li, Y.; Wang, C.; Sun, Y.; He, G.; Maurin, G.; Wang, S.; et al. Oriented titanium-MOF membrane for hydrogen purification. *Angew. Chem., Int. Ed. Engl.* **2025**, *64* (1), No. e202413701.

(53) Chen, S.; Sun, Y.; Chen, S.; Gao, Y.; Wang, F.; Li, H.; Liu, Y. Facile fabrication of a highly (110)-oriented ZIF-7 film with rod-shaped seeds. *Chem. Commun.* **2021**, *57* (17), 2128−2131.

(54) Sun, Y.; Song, C.; Guo, X.; Liu, Y. Concurrent manipulation of out-of-plane and regional in-plane orientations of NH2-UiO-66 membranes with significantly reduced anisotropic grain boundary and superior h2/CO2 separation performance. *ACS Appl. Mater. Interfaces* **2020**, *12* (4), 4494−4500.

(55) Cravillon, J.; Muenzer, S.; Lohmeier, S.; Feldhoff, A.; Huber, K.; Wiebcke, M. Rapid room-temperature synthesis and characterization of nanocrystals of a prototypical zeolitic imidazolate framework. *Chem. Mater.* **2009**, *21* (8), 1410−1412.

(56) Liu, Y.; Chen, S.; Ji, T.; Yan, J.; Ding, K.; Meng, S.; Lu, J.; Liu, Y. Room-temperature synthesis of zeolite membranes toward optimized microstructure and enhanced butane isomer separation performance. *J. Am. Chem. Soc.* **2023**, *145* (14), 7718−7723.

(57) Liu, Y.; Ding, K.; Fan, X.; Chen, S.; Meng, S.; Yan, J.; Gao, Y.; Lu, J.; Liu, Y. Fabrication of highly b-oriented MFI zeolite film over broad temperature window. *Chem. Eng. Sci.* **2024**, *293*, No. 120076.

(58) Li, D.; Ye, M.; Ma, C.; Li, N.; Gu, Z.; Qiao, Z. Preparation of a self-supported zeolite glass composite membrane for CO2 /CH4 separation. *Smart Molecules* **2024**, *2* (3), No. e20240009.

(59) Wu, M.; Yan, J.; Ji, T.; Yu, K.; Sun, Y.; Liu, Y.; Bai, X.; Liu, Y.; Liu, J.; Ma, J.; et al. Synthesis of (222)-oriented defect-rich MOF-808 membranes towards high-efficiency uranium rejection. *J. Membr. Sci.* **2025**, *717*, No. 123570.

(60) Wang, Z.; Huang, L.; Dong, X.; Wu, T.; Qing, Q.; Chen, J.; Lu, Y.; Xu, C. Ion sieving in graphene oxide membrane enables efficient actinides/lanthanides separation. *Nat. Commun.* **2023**, *14* (1), 261.

(61) Liu, X.; Demir, N. K.; Wu, Z.; Li, K. Highly water-stable zirconium metal-organic framework UiO-66 membranes supported on alumina hollow fibers for desalination. *J. Am. Chem. Soc.* **2015**, *137* (22), 6999−7002.

(62) Yao, Y.; Liao, J.; Xu, X.; Huang, C.; Fu, M.; Chen, K.; Ma, L.; Han, J.; Xu, L.; Ma, H. Hydrazide and amidoxime dual functional membranes for uranium extraction from seawater. *J. Mater. Chem. A* **2024**, *12* (17), 10528−10538.

(63) Hao, M.; Xie, Y.; Liu, X.; Chen, Z.; Yang, H.; Waterhouse, G.; Ma, S.; Wang, X. Modulating uranium extraction performance of multivariate covalent organic frameworks through donor-acceptor linkers and amidoxime nanotraps. *JACS Au* **2023**, *3* (1), 239−251.